Collective spontaneous emission beyond the rotating-wave approximation

Yong Li,[1,2] Jörg Evers,[1,2] Hang Zheng,[3] and Shi-Yao Zhu[1]
[1]*Beijing Computational Science Research Center, Beijing 100084, China*
[2]*Max-Planck-Institut für Kernphysik, Saupfercheckweg 1, 69117 Heidelberg, Germany*
[3]*Department of Physics, Shanghai Jiao Tong University, Shanghai 200030, China*
(Received 28 March 2012; published 22 May 2012)

The collective spontaneous emission of N multilevel atoms is studied in optical vector theory and without applying the rotating-wave approximation. The counter-rotating terms are included using a unitary transformation method. We analyze the decay dynamics starting from two initial conditions, the standard Dicke and timed Dicke states. In addition to the dependence on ensemble volume and density, we also study the effect of the ensemble geometry on cooperative emission for spheres, cubes, and quasi-two-dimensional shapes in different orientations. Finally, time-dependent cooperative spontaneous emission rates are introduced and investigated.

DOI: 10.1103/PhysRevA.85.053830 PACS number(s): 42.50.Nn, 42.50.Ct, 03.65.Yz

I. INTRODUCTION

The phenomenon of spontaneous emission from atomic systems is one of the most intriguing effects in quantum optics. Spontaneous emission and the Lamb shift are not immutable properties of the atom itself, but also depend on external influences such as the environment [1]. In a pioneering work by Dicke [2], it was found that the spontaneous emission from an ensemble of two-level atoms confined inside a volume of dimensions much smaller or much larger than the involved emission wavelength is modified by collective effects. The emission can either be accelerated (superradiance) or slowed down (subradiance) compared to the natural decay time scale. Subsequently, superradiance and subradiance were extensively studied theoretically and experimentally [3–22]. In most theoretical studies, the rotating-wave approximation (RWA) is applied to simplify the discussion. Then the atomic system can be reduced to a small number of states, as counter-rotating contributions to the Hamiltonian leading to evolutions to higher excited states are neglected [14–18]. It is commonly assumed that the RWA is a reasonably good approximation as the counter-rotating terms formally violate energy conservation, leading to virtual processes, and thus are suppressed. Recently, Scully and co-workers [19,20] and Friedberg and Manasseh [21] discussed the collective spontaneous emission of N two-level atoms with the counter-rotating terms included. Surprisingly, it was found that the virtual processes from the counter-rotating terms could induce non-negligible effects in the long-time cooperative spontaneous emission.

Recently, an alternative method based on unitary transformations was introduced to include the effects of the counter-rotating terms [23] for the case of a single multilevel atom. It was found that the time evolution of the spontaneous emission at short times is different from that obtained with the RWA, which could be interpreted in terms of the quantum Zeno [24] and anti-Zeno effects [25]. A similar method was later used [26–35] to consider both the short-time and the long-time spontaneous emission behavior for a two-level or multilevel atom either in vacuum or in other reservoirs with different spectra. The method has also been used [36] to study the Lamb shift [37] and emission spectra of spontaneous emission of two identical multilevel atoms. The unitary transformation method has three major advantages: (1) After the unitary transformation, the effective Hamiltonian has the form of an RWA Hamiltonian, even though the RWA is not applied. (2) The self-energy of the electron can be subtracted from the Hamiltonian at the beginning. (3) The full level structure of the original atom can easily be considered [28]. This is crucial, as with counter-rotating terms included, the original atom can no longer be modeled as a two-level system. The reason is that the influence of other levels is of the same order in the counter-rotating terms.

In this paper, we study the collective spontaneous emission of N *multilevel* atoms in vacuum. We consider two initial states with one excitation coherently spread out over many atoms and zero photons in the reservoir: first, the standard Dicke state, and, second, the timed Dicke state [17,19]. As the polarization and the vector character of the fields are important in the study of the collective spontaneous emission, we use a vector theory including all possible wave-vector directions and polarizations of the vacuum modes in the three-dimensional space. For low atomic density, the correlations between the atoms are negligible, while for very small volumes with large density ($V \ll \lambda^3$ with λ the involved optical wavelength), the standard Dicke state and the timed Dicke state coincide. Therefore, we mainly focus on intermediate densities in the range of 10 atoms/λ^3. Note that the decay dynamics depends on the spatial structure of the atoms, as well as on the initial state (the relative phases between atoms), as it is the superposition of one excitation in a large number of atoms. This excitation involves all atoms coherently, so that all atoms take part in the system's time evolution. The relative phases between the atoms are important. For the standard Dicke state, the relative phases are zero, while for the timed Dicke state, the relative phases depends on the distance between the atoms and the wave vector of the exciting field. Our main observables are the population in the initial state, the total population in atomic excited states, and the cooperative decay rates. We find that, as expected, both the timed and the standard Dicke initial states form approximately exponentially decaying eigenstates of the ensemble for small volumes. But for intermediate volumes, they are not eigenstates of the ensemble, resulting in complex time evolutions of the initial excitation. Next, we consider the effect of the ensemble geometry on the cooperative emission. We find that at intermediate sizes, the emission dynamics depends on the shape of the ensemble, which can

be interpreted as arising from the geometry dependence of the cooperative Lamb shift. After a comparison of a sphere to a cube, we also analyze quasi-two-dimensional samples in different orientations, and find characteristic differences in the dependence on the geometry for timed and regular Dicke states. We further analyze the dependence of the emission dynamics of the timed Dicke state on the relative orientation of the atomic dipole moments to the wave vector of the exciting photon. Finally, we introduce the time-dependent cooperative emission rate in order to describe the emission dynamics for intermediate ensemble volumes, and study its time evolution.

II. MODEL AND HAMILTONIAN

We consider N identical multilevel atoms interacting with the electromagnetic vacuum field. The total Hamiltonian of the system reads ($\hbar = 1$)

$$H = \sum_j \sum_l \omega_l \left|l\right\rangle_{jj} \left\langle l\right| + \sum_{\mathbf{k}} \omega_{\mathbf{k}} b_{\mathbf{k}}^\dagger b_{\mathbf{k}} + \sum_{j,\mathbf{k}} \sum_{l,m} g_{\mathbf{k},lm} \left|l\right\rangle_{jj} \left\langle m\right| (b_{\mathbf{k}}^\dagger e^{-i\mathbf{k}\cdot\mathbf{r}_j} + \text{H.c.}), \quad (1)$$

where ω_l is the energy of the level $|l\rangle$, $b_{\mathbf{k}}$ ($b_{\mathbf{k}}^\dagger$) is the creation (annihilation) operator of the $\mathbf{k}$th-mode vacuum field of frequency $\omega_{\mathbf{k}}$ and wave vector $\mathbf{k}$, $\mathbf{r}_j$ is the position of the jth atom, and

$$g_{\mathbf{k},lm} = |\omega_{lm}| d_{lm} \sqrt{\frac{1}{2\epsilon_0 \omega_{\mathbf{k}} V}} (\hat{d}_{lm} \cdot \hat{e}_{\mathbf{k}}) \quad (2a)$$

$$:= g_{k,lm} (\hat{d}_{lm} \cdot \hat{e}_{\mathbf{k}}) \quad (2b)$$

is the coupling strength. Here $\hat{e}_{\mathbf{k}}$ is the polarization direction of the $\mathbf{k}$th-mode field such that $\hat{e}_{\mathbf{k}} \cdot \mathbf{k} = 0$. Usually, there are two polarizations for each optical mode. But throughout this paper, we consider only one of the two, $\hat{e}_{\mathbf{k}}$, which is in the plane spanned by $\mathbf{d}_{lm}$ and $\mathbf{k}$, and neglect the other one, $\hat{e}'_{\mathbf{k}}$, which is normal to both $\mathbf{d}_{lm}$ and $\mathbf{k}$ and brings no contribution. We assume that the dipole moments of all atoms are aligned, such that the dipole moment $\mathbf{d}_{lm} \equiv d_{lm}\hat{d}_{lm}$ for the transition between the levels $|l\rangle$ and $|m\rangle$ is identical for all the atoms. For the sake of simplicity, we can further assume that $g_{\mathbf{k},lm}$ is real. Note that $g_{\mathbf{k},lm} = 0$ for $l = m$, and we define the notations $\mathbf{r}_{jj'} \equiv \mathbf{r}_j - \mathbf{r}_{j'}$ and $\omega_{lm} \equiv \omega_l - \omega_m$.

Next, we introduce a unitary transformation $U = \exp(iS)$ with

$$S = \sum_{j,\mathbf{k}} \sum_{l,m} \frac{g_{\mathbf{k},lm}\xi_{\mathbf{k},lm}}{i\omega_{\mathbf{k}}} \left|l\right\rangle_{jj} \left\langle m\right| (b_{\mathbf{k}}^\dagger e^{-i\mathbf{k}\cdot\mathbf{r}_j} - \text{H.c.}) \quad (3)$$

and

$$\xi_{\mathbf{k},lm} = \frac{\omega_{\mathbf{k}}}{\omega_{\mathbf{k}} + |\omega_{lm}|}. \quad (4)$$

Subtracting in addition the free-electron self-energy

$$E_{\text{self}} = -\sum_{j,\mathbf{k}} \sum_{l,m} \frac{|g_{\mathbf{k},lm}|^2}{\omega_{\mathbf{k}}} \left|l\right\rangle_{jj} \left\langle l\right|, \quad (5)$$

the effective Hamiltonian after the transformation can be written as

$$H^S = U^\dagger H U - E_{\text{self}} = H_0^S + H_1 + H_{V1} + H_{V2} + O(g^2). \quad (6)$$

In the above expression, we have expanded the Hamiltonian in powers of $g_{\mathbf{k},lm}$. The zeroth-order term evaluates to

$$H_0^S = \sum_{\mathbf{k}} \omega_{\mathbf{k}} b_{\mathbf{k}}^\dagger b_{\mathbf{k}} + \sum_j \sum_l \omega'_l \left|l\right\rangle_{jj} \left\langle l\right|, \quad (7)$$

where we have introduced the effective state energies $\omega'_l = \omega_l + \delta_l$ with

$$\delta_l = -\sum_{m,\mathbf{k}} \frac{|g_{\mathbf{k},lm}|^2}{\omega_{\mathbf{k}}} \left(2\xi_{\mathbf{k},lm} - \xi_{\mathbf{k},lm}^2 + \frac{\omega_{lm}}{\omega_{\mathbf{k}}}\xi_{\mathbf{k},lm}^2 - 1\right). \quad (8)$$

Here, the energy shift δ_l can be interpreted as the single-atom nondynamic Lamb shift [28] for level $|l\rangle$ as it is not related to any decay process.

The first-order term of the Hamiltonian (6) can be expressed as

$$H_1 = \sum_{j,\mathbf{k}} \sum_{l>m} \frac{2g_{\mathbf{k},lm}|\omega_{lm}|}{\omega_{\mathbf{k}} + |\omega_{lm}|} (\left|l\right\rangle_{jj} \left\langle m\right| b_{\mathbf{k}} e^{i\mathbf{k}\cdot\mathbf{r}_j} + \text{H.c.}), \quad (9)$$

and describes vacuum-induced transitions between the states. Note that Eq. (9) has the form of a Hamiltonian in the RWA, even though we did not apply the RWA to the original Hamiltonian Eq. (1). Instead, the simple structure of Eq. (9) originates from the unitary transformation Eq. (3).

The second-order terms in the Hamiltonian (6) are

$$H_{V1} = -\sum_{j,\mathbf{k}} \sum_{l,m,n\neq l} \frac{g_{\mathbf{k},lm}g_{\mathbf{k},mn}\xi_{\mathbf{k},lm}\xi_{\mathbf{k},mn}}{2\omega_{\mathbf{k}}^2} \left|l\right\rangle_{jj} \left\langle n\right| \times (2\omega_{\mathbf{k}} + 2|\omega_{lm}| + 2|\omega_{nm}| + \omega_{lm} + \omega_{nm}), \quad (10)$$

$$H_{V2} = -\sum_{j\neq j',\mathbf{k}} \sum_{l,l',m,m'} \frac{g_{\mathbf{k},lm}g_{\mathbf{k},l'm'}\xi_{\mathbf{k},lm}}{2\omega_{\mathbf{k}}} (2 - \xi_{\mathbf{k},l'm'}) \times (e^{i\mathbf{k}\cdot\mathbf{r}_{jj'}} + \text{c.c.}) \left|l\right\rangle_{jj} \left\langle m\right| \otimes \left|l'\right\rangle_{j'j'} \left\langle m'\right|. \quad (11)$$

They arise due to virtual photon processes involving the emission and reabsorption of a photon related to the counter-rotating terms in Eq. (1). The term H_{V1} describes virtual photon processes within the same atom, whereas H_{V2} describes virtual photon processes between two different atoms.

In the interaction picture with respect to H_0^S, the interaction Hamiltonian becomes

$$H_I = e^{iH_0^S t}(H_1 + H_{V1} + H_{V2})e^{-iH_0^S t} = H_1^I + H_{V1}^I + H_{V2}^I, \quad (12)$$

where

$$H_1^I = e^{iH_0^S t} H_1 e^{-iH_0^S t} = \sum_{j,\mathbf{k}} \sum_{l>m} \frac{2g_{\mathbf{k},lm}|\omega_{lm}|}{\omega_{\mathbf{k}} + |\omega_{lm}|} \times (\left|l\right\rangle_{jj} \left\langle m\right| e^{i\omega'_{lm}t} b_{\mathbf{k}} e^{-i\omega_{\mathbf{k}}t} e^{i\mathbf{k}\cdot\mathbf{r}_j} + \text{H.c.}), \quad (13a)$$

$$H_{V1}^I = e^{iH_0^S t} H_{V1} e^{-iH_0^S t}$$
$$= -\sum_{j,\mathbf{k}} \sum_{l,m,n\neq l} \frac{g_{\mathbf{k},lm} g_{\mathbf{k},mn} \xi_{\mathbf{k},lm} \xi_{\mathbf{k},mn}}{2\omega_{\mathbf{k}}^2} e^{i\omega'_{ln} t}$$
$$\times (2\omega_{\mathbf{k}} + 2|\omega_{lm}| + 2|\omega_{nm}| + \omega_{lm} + \omega_{nm}) |l\rangle_{jj}\langle n|, \tag{13b}$$

$$H_{V2}^I = e^{iH_0^S t} H_{V2} e^{-iH_0^S t}$$
$$= -\sum_{j\neq j',\mathbf{k}} \sum_{l,l',m,m'} \frac{g_{\mathbf{k},lm} g_{\mathbf{k},l'm'} \xi_{\mathbf{k},lm}}{2\omega_{\mathbf{k}}} (2 - \xi_{\mathbf{k},l'm'})$$
$$\times |l\rangle_{jj}\langle m| e^{i\omega'_{lm} t} \otimes |l'\rangle_{j'j'}\langle m'|$$
$$\times e^{i\omega'_{l'm'} t} (e^{i\mathbf{k}\cdot\mathbf{r}_{jj'}} + \text{c.c.}). \tag{13c}$$

III. TIME EVOLUTION FOR SINGLE-ATOM-EXCITATION STATES

A. Equations of motion

We next consider the special case of a single excitation distributed in the ensemble of atoms. We denote the ground and first excited levels of the individual atoms as $|g\rangle$ and $|e\rangle$, respectively. The ensemble ground state of H_0^S then is

$$|G_0\rangle := |G,\mathbf{0}\rangle = |g_1 g_2 \cdots g_N\rangle\,|\mathbf{0}\rangle\,, \tag{14}$$

with $|\mathbf{0}\rangle$ being the vacuum state of the electromagnetic field. The single-atom excited states of the system can be expressed as superpositions of basis states ($j \in \{1,\ldots,N\}$)

$$|e_j\rangle := |g_1 g_2 \cdots e_j \cdots g_N\rangle. \tag{15}$$

Finally, we denote the state with all atoms in the ground state and a single photon in mode $\mathbf{k}$ as $|G,1_{\mathbf{k}}\rangle = |G\rangle|1_{\mathbf{k}}\rangle$.

From the structure of the effective Hamiltonian, Eqs. (13), it is clear that when we start with the single-atom first excited state, the influence of the higher excited states is at the fourth order of the coupling constant, which can be neglected, so that the higher excited levels can be discarded. Therefore, the single-excitation states ($|e_j\rangle$ and $|G,1_{\mathbf{k}}\rangle$) span the sub-Hilbert space relevant for the dynamics of the system with initially one excitation in the atoms.

In the following, we will consider two types of initial state of the atoms, the standard Dicke state [2]

$$|D\rangle = \frac{1}{\sqrt{N}} \sum_j |e_j,\mathbf{0}\rangle, \tag{16}$$

and the timed Dicke states [17,19]

$$|T_{\mathbf{k}_l}\rangle = \frac{1}{\sqrt{N}} \sum_j e^{i\mathbf{k}_l\cdot\mathbf{r}_j} |e_j,\mathbf{0}\rangle. \tag{17}$$

Here, $\mathbf{k}_l$ is the wave vector of the single photon field which prepared the state and thus defined the relative phase of the different excitation possibilities. Note that there is a nondynamic shift δ_e [as in Eq. (8)] for these two initial states coming from H_0^S due to the counter-rotating terms, which is the same for the above two initial single-excitation states [23,28].

The single-excitation wave function in the interaction picture can be written as

$$|\psi(t)\rangle = \sum_j \beta_j(t) |e_j,\mathbf{0}\rangle + \sum_{\mathbf{k}} \eta_{\mathbf{k}}(t)\,|G,1_{\mathbf{k}}\rangle\,. \tag{18}$$

This simple structure is in contrast to the formulation in terms of the original Hamiltonian Eq. (1), which contains counter-rotating terms leading to higher excited states. Thus, due to the unitary transformation Eq. (3), the problem reduces to that of an ensemble of two-level atoms, even though (i) the modification to the energies of the lowest two levels from all the higher levels is included and (ii) the atom-atom interaction through virtual photons is included.

The time evolution of Eq. (18) follows the Schrödinger equation

$$i\,\partial_t\,|\psi(t)\rangle = H_I\,|\psi(t)\rangle\,, \tag{19}$$

which leads to the equations of motion for the state amplitudes

$$\dot\beta_j(t) = -i \sum_{\mathbf{k}} g_{\mathbf{k},eg} \frac{2\omega_{\text{eg}}}{\omega_{\mathbf{k}} + \omega_{\text{eg}}} e^{i\omega'_{\text{eg}} t} e^{-i\omega_{\mathbf{k}} t} e^{i\mathbf{k}\cdot\mathbf{r}_j} \eta_{\mathbf{k}}(t)$$
$$+ i \sum_{j'\neq j} \sum_{\mathbf{k}} \frac{g_{\mathbf{k},eg} g_{\mathbf{k},ge} \xi_{\mathbf{k},eg}}{\omega_{\mathbf{k}}} (2 - \xi_{\mathbf{k},ge})$$
$$\times (e^{i\mathbf{k}\cdot\mathbf{r}_{jJ}} + \text{c.c.}) \beta_{j'}(t), \tag{20}$$

$$\dot\eta_{\mathbf{k}}(t) = -i \sum_{j'} \frac{2 g_{\mathbf{k},eg} \omega_{\text{eg}}}{\omega_{\mathbf{k}} + \omega_{\text{eg}}} e^{-i(\omega'_{\text{eg}} - \omega_{\mathbf{k}})t} e^{-i\mathbf{k}\cdot\mathbf{r}_{j'}} \beta_{j'}(t). \tag{21}$$

Formal integration of Eq. (21) with the initial value $\eta_{\mathbf{k}}(0) = 0$ leads to

$$\eta_{\mathbf{k}}(t) = -i \sum_{j'} \frac{2\omega_{\text{eg}} g_{\mathbf{k},eg} e^{-i\mathbf{k}\cdot\mathbf{r}_{j'}}}{\omega_{\mathbf{k}} + \omega_{\text{eg}}}$$
$$\times \int_0^t e^{-i(\omega'_{\text{eg}} - \omega_{\mathbf{k}})t'} \beta_{j'}(t') dt'. \tag{22}$$

Substituting Eq. (22) into Eq. (20), and noting that in the Markov approximation and long-time limit $t \to \infty$,

$$\int_0^t e^{i(\omega'_{\text{eg}} - \omega_{\mathbf{k}})(t-t')} \beta_{j'}(t') dt'$$
$$\approx \beta_{j'}(t) \int_{-\infty}^t e^{i(\omega'_{\text{eg}} - \omega_{\mathbf{k}})(t-t')} dt'$$
$$= \beta_{j'}(t) \left[\pi\,\delta(\omega'_{\text{eg}} - \omega_{\mathbf{k}}) + i\,\text{P}\left(\frac{1}{\omega'_{\text{eg}} - \omega_{\mathbf{k}}} \right) \right]$$
$$= \beta_{j'}(t) \frac{i}{\omega'_{\text{eg}} - \omega_{\mathbf{k}} + i0^+}, \tag{23}$$

where P(·) stands for the principal value, one finds

$$\dot\beta_j(t) = -\frac{\Gamma_0}{2} \beta_j(t) - \sum_{j'(\neq j)} \frac{\Gamma_{j'}^{(j)}}{2} \beta_{j'}(t). \tag{24}$$

Here,

$$\Gamma_0 = 8\omega_{\text{eg}}^2 \sum_{\mathbf{k}} \frac{g_{\mathbf{k},eg}^2}{(\omega_{\mathbf{k}} + \omega_{\text{eg}})^2} \frac{i}{\omega'_{\text{eg}} - \omega_{\mathbf{k}} + i0^+} \tag{25}$$

is the complex single-atom decay rate which is identical for each atom. The second term

$$\begin{aligned}\Gamma_{j'}^{(j)} &= -i\sum_{\mathbf{k}} g_{\mathbf{k},eg}^2 \left[\frac{-8\omega_{\rm eg}^2 e^{i\mathbf{k}\cdot\mathbf{r}_{jj'}}}{(\omega_{\mathbf{k}}+\omega_{\rm eg})^2}\frac{1}{\omega'_{\rm eg}-\omega_{\mathbf{k}}+i0^+}\right.\\ &\left.+\frac{2\xi_{\mathbf{k},eg}}{\omega_{\mathbf{k}}}(2-\xi_{\mathbf{k},ge})(e^{i\mathbf{k}\cdot\mathbf{r}_{jj'}}+\text{c.c.})\right]\\ &\approx 2i\sum_{\mathbf{k}} g_{\mathbf{k},eg}^2\cos(\mathbf{k}\cdot\mathbf{r}_{jj'})\\ &\times\left(\frac{1}{\omega_{\rm eg}-\omega_{\mathbf{k}}+i0^+}-\frac{1}{\omega_{\rm eg}+\omega_{\mathbf{k}}+i0^+}\right)\end{aligned} \tag{26}$$

describes the interaction between two different atoms j and j'. Note that we approximated $\omega'_{\rm eg}\approx\omega_{\rm eg}$ in the final step in Eq. (26). This introduces an error proportional to g^4 and therefore has a negligible effect on the value of $\Gamma_{j'}^{(j)}$ (or Γ_0) [28]. A detailed calculation in the Appendix yields

$$\Gamma_0=\gamma_0-i\frac{2\gamma_0}{\pi}, \tag{27}$$

where $\gamma_0=k_{\rm eg}^3 d_{\rm eg}^2/(3\pi\epsilon_0)$ is the standard single-atom spontaneous emission rate in vector theory [38]. The term $-\gamma_0/\pi$ $(=: L_0)$ coming from the imaginary part is the single-atom dynamic Lamb shift [39]. Note that the single-atom (half-)decay rate γ_s in scalar photon theory [19,20] is different from the result for vector theory, as $\gamma_s=k_{\rm eg}^3 d_{\rm eg}^2/(2\pi\epsilon_0)$.

Similarly, $\Gamma_{j'}^{(j)}$ in Eq. (26) can be evaluated to

$$\Gamma_{j'}^{(j)}=\sin^2\theta_{jj'}\Gamma_{j',1}^{(j)}+\frac{(3\cos^2\theta_{jj'}-1)}{2}\Gamma_{j',2}^{(j)}, \tag{28}$$

where

$$\Gamma_{j',1}^{(j)}=-i\frac{3\exp(i\zeta_{jj'})}{2\zeta_{jj'}}\gamma_0 \tag{29}$$

is proportional to the induced term in scalar photon theory [see Eq. (A7) in Ref. [20]], and

$$\begin{aligned}\Gamma_{j',2}^{(j)}=&\frac{3}{\zeta_{jj'}^3}\gamma_0[(\sin\zeta_{jj'}-\zeta_{jj'}\cos\zeta_{jj'})\\ &+i(1-\cos\zeta_{jj'}-\zeta_{jj'}\sin\zeta_{jj'})]\end{aligned} \tag{30}$$

with $\zeta_{jj'}:=k_{\rm eg}r_{jj'}\equiv\omega_{\rm eg}r_{jj'}/c$. Note that $\theta_{jj'}$ is the angle between $\hat{d}_{\rm eg}$ and $\mathbf{r}_{jj'}$, and we have assumed the dipole moments of the atoms to be aligned along the z direction ($\hat{d}_{\rm eg}=\hat{e}_z$).

B. Eigensystem analysis

After having established the equations of motions Eq. (24) for the state coefficients β_j, the problem of the time evolution of cooperative spontaneous emission of N atoms reduces to finding all eigenstates $\overrightarrow{\boldsymbol{\beta}}^{(n)}$ and complex eigenvalues λ_n of the evolution matrix, as in [20]. The time evolution in such an eigenstate is given by

$$\overrightarrow{\boldsymbol{\beta}}^{(n)}(t)=\overrightarrow{\boldsymbol{\beta}}^{(n)}e^{-\lambda_n t}, \tag{31}$$

where $\overrightarrow{\boldsymbol{\beta}}^{(n)}\equiv(\beta_1^{(n)},\beta_2^{(n)},\ldots,\beta_N^{(n)})$ and $\mathrm{Re}(\lambda_n)>0$ is the decay rate of the eigenstate. Substituting this ansatz into Eq. (24) yields the secular equation

$$\lambda_n\overrightarrow{\boldsymbol{\beta}}^{(n)}=\overrightarrow{\boldsymbol{\beta}}^{(n)}\boldsymbol{\Gamma}, \tag{32}$$

where the matrix element of $\boldsymbol{\Gamma}$ is

$$\boldsymbol{\Gamma}_{jj'}=\begin{cases}\Gamma_0/2 & \text{for } j=j',\\ \Gamma_{j'}^{(j)}/2 & \text{for } j\neq j'.\end{cases} \tag{33}$$

Technically, $\overrightarrow{\boldsymbol{\beta}}^{(n)}$ is the left eigenvector of the symmetric and non-Hermitian matrix $\boldsymbol{\Gamma}$ which is the effective Hamiltonian describing the time evolution of the singly excited atoms, and λ_n is the corresponding complex eigenvalue. One can also write the secular equation as

$$\lambda_n(\overrightarrow{\boldsymbol{\beta}}^{(n)})^T=\boldsymbol{\Gamma}(\overrightarrow{\boldsymbol{\beta}}^{(n)})^T, \tag{34}$$

where $(\overrightarrow{\boldsymbol{\beta}}^{(n)})^T=(\beta_1^{(n)},\beta_2^{(n)},\ldots,\beta_N^{(n)})^T$ is the right eigenvector of $\boldsymbol{\Gamma}$. Here T denotes the transpose. That is, the symmetric non-Hermitian matrix $\boldsymbol{\Gamma}$ can be diagonalized as

$$\boldsymbol{\Gamma}=\sum_{n=1}^{N}\lambda_n(\overrightarrow{\boldsymbol{\beta}}^{(n)})^T\overrightarrow{\boldsymbol{\beta}}^{(n)} \tag{35}$$

with $\overrightarrow{\boldsymbol{\beta}}^{(n)}$ satisfying $\overrightarrow{\boldsymbol{\beta}}^{(m)}(\overrightarrow{\boldsymbol{\beta}}^{(n)})^T=\delta_{mn}$.

After obtaining the eigenvalues and eigenvectors from the secular equation (by numerical calculation), one can consider the time evolution of an arbitrary initial single-atom-excitation state $|\psi(0)\rangle$. For this, the initial state is decomposed into a superposition of eigenstates $|\lambda_n\rangle$ corresponding to $(\overrightarrow{\boldsymbol{\beta}}^{(n)})^T$ as

$$|\psi(0)\rangle=\sum_{n=1}^{N}a_n|\lambda_n\rangle, \tag{36}$$

such that its time evolution is

$$|\psi(t)\rangle=\sum_{n}a_n e^{-\lambda_n t}|\lambda_n\rangle. \tag{37}$$

If one of the a_n's dominates the initial state, then the initial state $|\psi(0)\rangle$ is an approximate (exponentially decaying) eigenstate. Otherwise, $|\psi(0)\rangle$ is not an eigenstate, such that the time evolution is a superposition of different exponentially decaying components.

We start by analyzing the eigenvalue structure of the system, which is dependent on the atom number and volume, but is independent of the initial state of the single-atom excitation. We consider two ensemble shapes, a cube and a sphere, for an intermediate volume $V=(5\lambda)^3$ and a small volume $V=(0.1\lambda)^3$ with the same atom density. There are $N=8000$ atoms randomly distributed in the cubes or spheres. In Figs. 1(a) and 1(b), we plot eigenvalues for $V=(5\lambda)^3$ and $V=(0.1\lambda)^3$, respectively. The eigenvalues are arranged in the order of decreasing real part.

It can be seen that the real and imaginary parts of the eigenvalues for the sphere and the cube with the same volume (as well as the same density) are similar. However, a difference for the eigenvalues with largest real parts can be observed in the intermediate-volume case as shown the inset of Fig. 1(a). Thus we find that a sphere gives rise to faster decay in the case of superradiance. This can be viewed as a manifestation of the shape dependence of the cooperative superradiance. For small

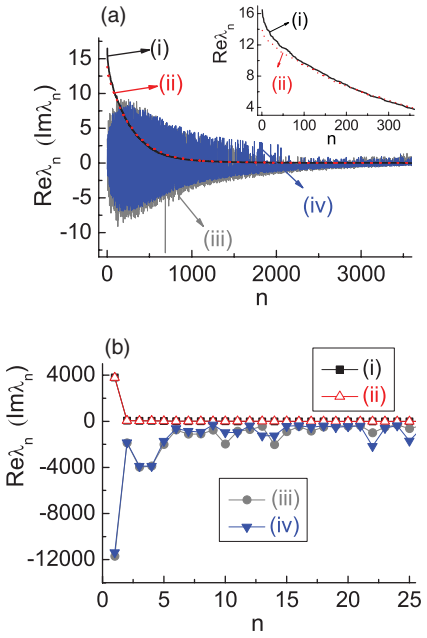

FIG. 1. (Color online) Real [curves (i) and (ii)] and imaginary [curves (iii) and (iv)] parts of the eigenvalues (in units of γ_0). Results are shown for an ensemble of $N = 8000$ atoms (a) in an intermediate volume $V = (5\lambda)^3$ and (b) in a small volume $V = (0.1\lambda)^3$. Note that (ii) and (iv) show the results for a cube, whereas (i) and (iii) show those of a sphere of equal volume.

volumes, the real part of the first eigenvalue is much larger than the others; see Fig. 1(b). This is the dominant superradiant decay mode with half-decay rate approaching $N\gamma_0/2$. This is the expected behavior of Dicke superradiance for volumes much smaller than the typical optical wavelength [2]. In contrast to the intermediate-volume case, the results for the sphere and the cube of small volume are almost the same, as the cube and the sphere have no difference perceptible to the optical fields in this case. As will be discussed further in the following, in the intermediate-volume case, the decay rates can also scale with the number of atoms N, even though the absolute rates are smaller than in the small-volume case.

C. Observables

Next, we discuss the observables analyzed in the following. To characterize the ensemble state, we calculate the time-dependent population in the initial state

$$P^{(I)}(t) = |\langle\psi(0)\,|\psi(t)\rangle|^2\,, \tag{38}$$

and the total population in all atomic excited states

$$P^{(T)}(t) = \sum_j \langle e_j;\mathbf{0}\,|\psi(t)\rangle\,\langle\psi(t)\,|e_j;\mathbf{0}\rangle. \tag{39}$$

Here, the superscript "(I)" stands for the initial state and the superscript "(T)" for the total (atomic) excitation. Note that $P^{(I)}(t)$ and $P^{(T)}(t)$ differ, if the initial state is not an eigenstate of the system. Then, transitions between the different excited atomic states of the system occur, which change $P^{(I)}(t)$, but not $P^{(T)}(t)$.

The time-evolved state $|\psi(t)\rangle$ in Eq. (37) can also be written as

$$|\psi(t)\rangle = c_I(t)\,|\psi(0)\rangle + \sum_{\alpha=1}^{N-1} c_\alpha(t)\,|\psi_\alpha\rangle\,, \tag{40}$$

where the $|\psi_\alpha\rangle$ form a basis of the single-atom-excitation states orthogonal to $|\psi(0)\rangle$, such that $\langle\psi(0)|\psi_\alpha\rangle = 0$ for $\alpha \in \{1,\ldots,N-1\}$. (The specific form of $|\psi_\alpha\rangle$ is not of relevance here.) In this notation, the observables can be written as

$$P^{(I)}(t) = |\langle\psi(0)\,|\psi(t)\rangle|^2 = |c_I(t)|^2 \tag{41}$$

and

$$P^{(T)}(t) = P^{(I)}(t) + \sum_\alpha |c_\alpha(t)|^2 \geqslant P^{(I)}(t). \tag{42}$$

Note that as the initial state is a subset of all single-atom-excitation states, one always has $P^{(I)}(t) \leqslant P^{(T)}(t)$.

We can further write

$$c_I(t) = \exp\left[-\frac{\gamma^{(I)}_{\rm eff}(t)}{2}t - iL^{(I)}_{\rm eff}(t)t - iL_0 t\right], \tag{43}$$

which defines the time-dependent effective decay rate $\gamma^{(I)}_{\rm eff}(t)$ and the time-dependent effective collective dynamical Lamb shift $L^{(I)}_{\rm eff}(t)$ of the initial state, respectively. Note that here we have extracted the single-atom dynamic shift L_0 $(= -\gamma_0/\pi)$ from the collective one. From this definition we find

$$P^{(I)}(t) = \exp\big[-\gamma^{(I)}_{\rm eff}(t)t\big]. \tag{44}$$

Similarly, we can also define a corresponding time-dependent effective decay rate $\gamma^{(T)}_{\rm eff}(t)$ for the total excitation of the system, such that

$$P^{(T)}(t) = \exp\big[-\gamma^{(T)}_{\rm eff}(t)t\big]. \tag{45}$$

IV. NUMERICAL ANALYSIS OF COLLECTIVE SPONTANEOUS EMISSION

A. Time evolution of the timed Dicke state

First, we consider the dependence of the evolution of a timed Dicke state $|T_{\mathbf{k}_I}\rangle$ in Eq. (17) on the direction of the wave vector of the preparing photon $\mathbf{k}_I$. For this, we analyze a spherical volume $V = \frac{4\pi}{3}(4\lambda)^3$ containing $N = 7000$ atoms. The wave number is chosen as $|\mathbf{k}_I| = k_{\rm eg}$, and we denote the angle between $\mathbf{k}_I$ and the dipole moment $\mathbf{d}_{\rm eg}$ (assumed along $\hat{e}_z$) as the incident angle θ_I. The results are shown Fig. 2. Figure 2(a) shows the time evolution of the total upper-state population with incident angles $\theta_I = 30^\circ$, 90°, and 170°, respectively. It can be seen that the time evolution strongly depends on the direction of the preparing field, which determines the relative phases entering the initial state. The decay of the total upper-state population for an initial timed Dicke state is fastest when the wave vector of the preparing field is normal to the direction of the atomic dipole moment, i.e., for incident angle close to 90°. Instead, when the wave vector of the preparing field is along the direction of the atomic dipole (that is, θ_I close to 180° or 0°), the system decays slowly. For comparison, the evolution for the Dicke state $|D\rangle$ is also

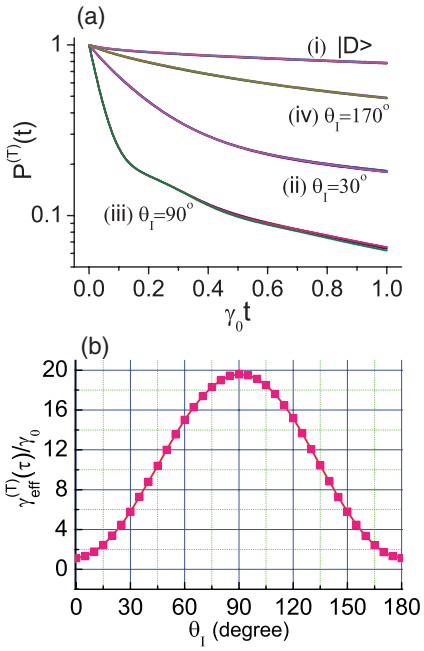

FIG. 2. (Color online) (a) Time evolution of the total upper-state population for different initial states. Curve (i) shows the results for the untimed standard Dicke state $|D\rangle$, and (ii)–(iv) for timed Dicke states with different incident angles θ_I of the preparing wave vector relative to the atomic dipole moments. The wave number of the preparing initial field is chosen as $|\mathbf{k}_I| \equiv k_{\rm eg}$. Each case (i)–(iv) shows the results for five realizations of atom positions in the volume, which lie on top of each other. (b) The effective decay rate for the total excitation at short time instant τ, $\gamma_{\rm eff}^{(T)}(\tau)$ as functions of the incident angle θ_I. The curve is an average over five realizations of the atom positions. In both panels, $N = 7000$ atoms are distributed randomly in a sphere of volume $V = 4\pi(4\lambda)^3/3$.

plotted [see curve (i) in Fig. 2(a)], which tells us that the standard Dicke state has the slowest decay.

To analyze the angle dependence further, we concentrate on the effective decay rate for the total upper-state population at short times τ (but still in the Markovian time limit, that is, $\gamma_0/\omega_{\rm eg} \ll \gamma_0\tau \ll 1$), $\gamma_{\rm eff}^{(T)}(\tau)$, as functions of the incident angle of $\mathbf{k}_I$. The results are shown in Fig. 2(b). Again, we find that the effective decay rate is fastest when the initial state is timed orthogonal to the dipole moment. An intuitive explanation for this relies on the fact that the superradiant emission of a timed Dicke state predominantly occurs in the forward direction, i.e., in the direction of the preparing field [19]. On the other hand, the dipole emission pattern has minima along the direction of the dipole moments. Therefore, fast superradiant decay can occur only if the emission direction imprinted on the ensemble matches the dipole emission pattern of the atoms. This result is obtained due to the vector nature of our calculation.

Our numerical calculations also show that the initial decay at very short times τ of the population in the initial state, $\gamma_{\rm eff}^{(I)}(\tau)$, coincides with the total decay rate $\gamma_{\rm eff}^{(T)}(\tau)$. This is consistent with the physical analysis from Eq. (42). At short times τ, the decay of the initial state to the ground state is proportional to τ: $[1 - |c_I(\tau)|^2] \propto \tau$. However, the transition of the initial state to other single-atom-excitation state is proportional to τ^2: $|c_\alpha(\tau)|^2 \propto \tau^2$. Thus, the initial decrease of the total upper-state population at the short-time instant τ is dominated by the decay of the initial atomic state to the atomic ground state. The transition of the initial state to other excited states becomes significant only later in the time evolution. Therefore, $\gamma_{\rm eff}^{(T)}(\tau) \approx \gamma_{\rm eff}^{(I)}(\tau)$ for short-time instant τ, such that the effective decay rates in Fig. 2(b) can directly be compared with the superradiant decay rates of the timed Dicke state predicted previously [19]. Moreover, Fig. 2(b) shows that $\gamma_{\rm eff}^{(T)}(\tau)$ is symmetric with respect to the angle of $\theta_I = 90^\circ$ at short-time instants τ, which also agrees with the theoretical analysis of the system's properties.

Finally, we note that Fig. 2 also illustrates the dependence of the results on the specific patterns of random atom positions in the chosen volume. There are five curves due to five different patterns for each incident field angle in Fig. 2(a), and the result in Fig. 2(b) is averaged over five different atom position patterns. It can be seen that an ensemble size of $N = 7000$ atoms is sufficient to average out statistical fluctuations, such that the different realizations lead to virtually indistinguishable results. In the following, results from single realizations of the random atom positions are shown, as averaging over several patterns would lead to similar results.

B. Time evolution of spherical ensembles

We now turn to the dependence of the dynamics of the timed Dicke state $|T\rangle = \sum_j e^{ik_{\rm eg}x_j}|e_j,\mathbf{0}\rangle/\sqrt{N}$ on the volume for intermediate atomic density. We consider $N = 8000$ atoms located randomly in spheres with different radii. The results are shown in Fig. 3, where (a) is for the total upper-state population $P^{(T)}(t)$, and (b) for the population in the initial state $P^{(I)}(t)$. The corresponding results for the time-dependent effective decay rates $\gamma_{\rm eff}^{(T)}(t)$ and $\gamma_{\rm eff}^{(I)}(t)$ are plotted in Figs. 3(c) and 3(d). Here and in the following, we set $\mathbf{k}_I = k_{\rm eg}\hat{e}_x$ in the case of the timed Dicke state.

One finds that for an initial timed Dicke state $|T\rangle$ in intermediate volumes, $P^{(T)}(t)$ always decreases with time, and the corresponding effective decay rates $\gamma_{\rm eff}^{(T)}(t)$ are larger than the single-atom rate γ_0 in the time interval $t \lesssim 1/\gamma_0$. Thus we find superradiance. Usually, the decay $\gamma_{\rm eff}^{(T)}(t)$ of $P^{(T)}(t)$ will decrease with time such that eventually subradiance occurs. In the long-time limit $t \to \infty$, $P^{(T)}(t) \propto \exp[-2{\rm Re}(\lambda_N)t]$, where ${\rm Re}(\lambda_N)$ (>0) is the smallest real part of the N complex eigenvalues in Eq. (32) and is much less than $\gamma_0/2$ for large N. This explains why $P^{(T)}(t)$ shows superradiance at first and then subradiance later [22].

The time evolution of $P^{(I)}(t)$ exhibits dips. The reason is that starting from an initial timed Dicke state, the system decays incoherently to the atomic ground state with generation of one photon, but also undergoes coherent transitions to other single-atom-excitation states, which can decay incoherently to the atomic ground state and evolve coherently to the initial state (also other single-atom-excitation states). At the beginning, the incoherent decay always dominates over the coherent transition back to the initial state and the related population projection on the initial state always decreases with time. After some time, the coherent transition back to the initial state may dominate over the incoherent decay, and the population in the

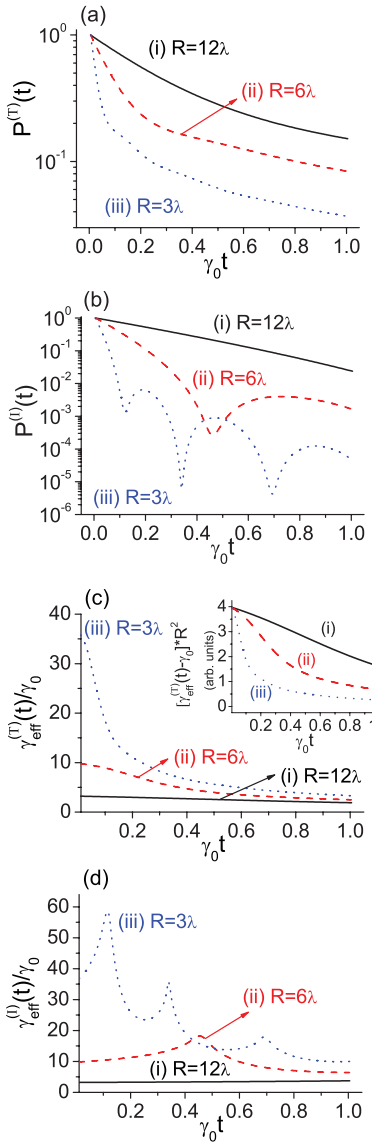

FIG. 3. (Color online) The dynamic evolution (a) of the total upper-state population $P^{(T)}(t)$ and (b) of the population in initial state $P^{(I)}(t)$, and (c) the corresponding effective decay rates $\gamma_{\rm eff}^{(T)}(t)$ and (d) $\gamma_{\rm eff}^{(I)}(t)$, with fixed $N = 8000$ atoms in a sphere of $V = 4\pi R^3/3$ with $R = 12\lambda$ (i), $R = 6\lambda$ (ii), or $R = 3\lambda$ (iii). Here the initial state is the timed Dicke state $|T\rangle = \sum_j e^{ik_{\rm eg}x_j}|e_j,\mathbf{0}\rangle/\sqrt{N}$.

initial state may increase. This happens in a limited period throughout the evolution.

We also see that in both cases the decay is faster with smaller radius as expected, since the effective interaction between the atoms becomes stronger and enhances the collective decay with decreasing radius. Similar results can also be obtained for other shapes of the atomic ensemble such as cubes. This is evidenced by the evolution of the population projection on the initial state, as the population minimum occurs at later times for larger volumes, which can be interpreted as slower population exchange between various excited states due to smaller interaction strength.

In the inset of Fig. 3(c), we plot the dynamic evolution of the collective decay rate (after subtracting the single-atom part), which shows that the collective decay rate is proportional to

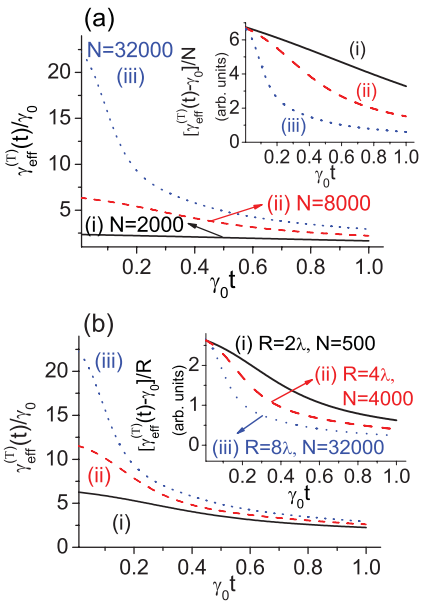

FIG. 4. (Color online) The effective decay rates of the total upper-state population (a) for different atom numbers (i) $N = 2000$, (ii) $N = 8000$, and (iii) $N = 32\,000$, and (b) for different spheres (different atom numbers) with fixed atomic density: (i) $R = 2\lambda$ and $N = 500$, (ii) $R = 4\lambda$ and $N = 4000$, and (iii) $R = 8\lambda$ and $N = 32\,000$. The insets are the corresponding collective decay rates scaled to the atom number [the inset in (a)] or scaled to the radius [the inset in (b)] in arbitrary units. Here the initial state is still the timed Dicke state $|T\rangle$ in Fig. 3.

R^{-2} throughout a short initial period. The dependence of the effective decay rate on the atom number N for fixed radius R is shown in Fig. 4(a), and the dependence on the radius R with fixed atomic density is shown in Fig. 4(b). Interestingly, we find that at the very beginning, the collective decay rate (after subtracting the single-atom part) divided by NR/V ($\propto N/R^2$) is constant, as shown by the insets of Figs. 3 and 4, which was predicted in Ref. [19]. At the beginning, the fast decay due to the eigenmodes, whose eigenvalues' real parts are large, dominates. Therefore, at the very beginning, the decay rate scales with the number of atoms as in the ordinary superradiance. Note that it also depends on the ensemble volume and shape. This scaling will not be observed at later times, because then the other eigenmodes, whose real parts of the eigenvalues are smaller, will dominate the decay. We observed such a scaling behavior at the very beginning also for other shapes such as cubes, but only when $N \gg 1$ and the dimension of the atomic ensemble is larger than λ. Otherwise, when the dimensions of the atomic ensemble are much smaller than λ, the well-known superradiance result is obtained wherein the collective decay rate for a standard Dicke state is proportional to N, independent of the atomic volume.

C. Time evolution of ensembles in quasi-two-dimensional cuboids

Next, we analyze the dynamics of atomic ensembles confined to a quasi-two-dimensional square sheet. The longer sides have length 10λ, and the thickness (short axis) is chosen as 0.01λ, resulting in a volume of $1\lambda^3$. In Fig. 5, we plot the

time evolution of the upper-state population for an initial timed Dicke state and the Dicke state for three different orientations (the short axis in the x, y, and z directions, respectively) and three different atom numbers (densities). The timed Dicke state $|T\rangle \equiv \sum_j e^{ik_{eg}x_j}|e_j,\mathbf{0}\rangle/\sqrt{N}$ is assumed to be initialized by a plane wave whose vector points in the x direction and whose polarization is parallel to the atomic dipoles (z direction). Due to the fixed directions of the wave vector and the dipoles, in general the evolutions in the three orientations are different from each other for a given initial state.

Now let us consider the effect of the orientation on the decay in detail. The slowest decay (subradiance) occurs in the case of an initial Dicke state $|D\rangle$ with the short axis of the cuboid along the z direction of the atomic dipoles [see Fig. 5(a)]. In this case, the position vectors connecting any two atoms are normal to the atomic dipoles, and the emission from a dipole is strongest in the direction normal to the dipole, which results in the strongest interference between atoms and the quenching of spontaneous emission. The decays of the initial Dicke state $|D\rangle$ in the cases of the two other orientations are faster [see Figs. 5(b) and 5(c)] and show superradiance, because some position vectors are not normal to the atomic dipoles. Note that the curve for $|D\rangle$ in Fig. 5(b) is the same as that in Fig. 5(c) for the same N. The decay of the timed Dicke state $|T\rangle$ with short axis along the incident wave vector (x direction) is the same as the decay of $|D\rangle$ with the short axis along the x orientation [see Fig. 5(c)], as $|T\rangle = |D\rangle$ in this orientation. In the two other orientations of the short axis (along the y and z directions), the decay dynamics of the timed Dicke states are similar [but not the same; see Figs. 5(a) and 5(b)], and are substantially different from the case of the short axis along the x orientation in Fig. 5(c). As expected, we find faster decay for higher densities. The detailed calculation (not shown in the figures here) shows that the collective decay rates for the superradiance in Fig. 5 are proportional to N at very short times, as discussed in Fig. 4(a) above.

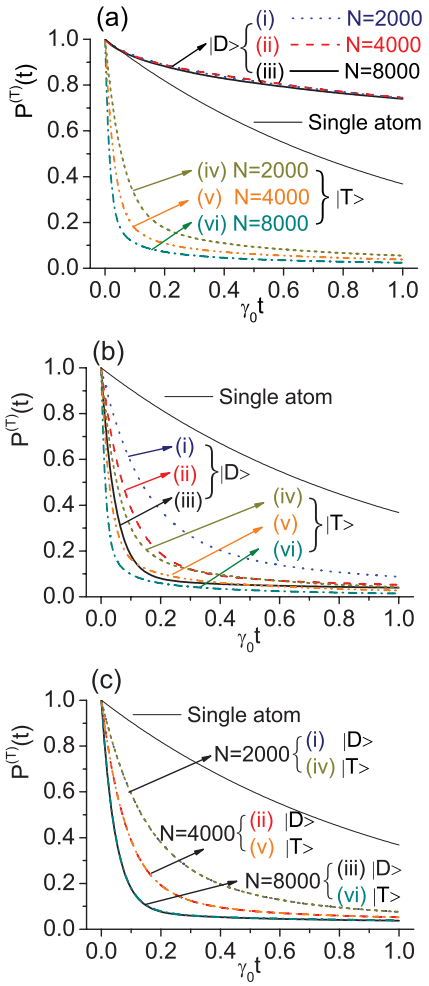

FIG. 5. (Color online) Time evolution of the total upper-state population $P^{(T)}(t)$ for the quasi-two-dimensional cuboid cases of (a) $V = 10\lambda \times 10\lambda \times 0.01\lambda$, (b) $V = 10\lambda \times 0.01\lambda \times 10\lambda$, and (c) $V = 0.01\lambda \times 10\lambda \times 10\lambda$. In all cases, curves (i)–(iii) stand for the initial standard Dicke state $|D\rangle$ and curves (iv)–(vi) for the timed Dicke state $|T\rangle = \sum_j e^{ik_{eg}x_j}|e_j,\mathbf{0}\rangle/\sqrt{N}$ [with curves (i) and (iv) $N = 2000$, curves (ii) and (v) $N = 4000$, and curves (iii) and (vi) $N = 8000$]. For comparison, the decay of a single atom is also plotted.

V. CONCLUSION

In conclusion, we investigated the collective spontaneous emission for N multilevel atoms in vacuum. We used the method of unitary transformations to include the counter-rotating terms in our analysis. We focused on the case with only one excitation initially in the atomic ensemble. Then, following the unitary transformation method, the system Hamiltonian assumes the simple RWA form for N two-level atoms, even though the RWA was not applied, and even though multilevel atoms are considered. The decay dynamics can then be studied by finding all eigenstates as well as their complex eigenvalues for an effective non-Hermitian matrix.

We analyzed the decay dynamics for different initial states chosen as timed Dicke states $|T_{\mathbf{k}_l}\rangle$ or untimed standard Dicke states $|D\rangle$, for different atom densities and different ensemble volumes and shapes. For this, we considered both the time evolution of the total upper-state population $[P^{(T)}(t)]$ and that of the population in the initial state $[P^{(I)}(t)]$.

Unlike some previous works based on the scalar optical feld theory, here, we considered all the directions and polarizations of the wave vectors for all the vacuum modes.

In the case of small volume, the timed Dicke state reduces to the standard Dicke state. Our numerical calculations show that then the timed or untimed Dicke states are approximately exponentially decaying eigenstates of the system. In this setup, superradiance appears with the effective decay rate increased by a factor of N.

However, in the intermediate-volume case, neither the standard Dicke state nor the timed Dicke state is an "eigen-state" of the system. Throughout their decay, the population in the initial state or all the upper states can exhibit both superradiance and subradiance. We found that for intermediate volumes, the emission dynamics depends on the shape of the ensemble, which can be interpreted as arising from the geometry dependence of the cooperative emission effect. After a comparison of a sphere to a cube, we also analyzed quasi-two-dimensional samples in different orientations, and found characteristic differences in the dependence on the geometry for timed and regular Dicke states. These effects arise

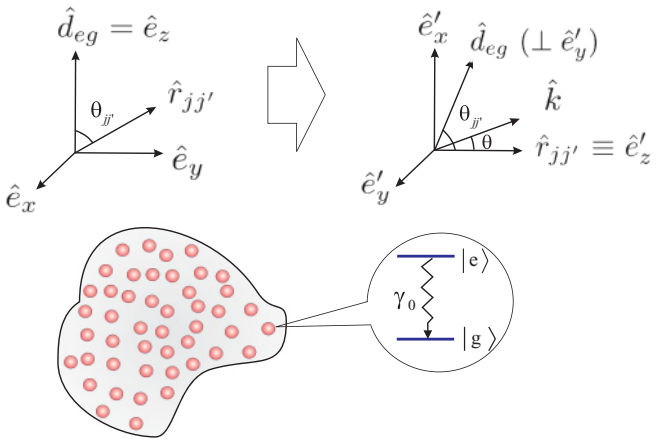

FIG. 6. (Color online) The ensemble of randomly distributed atoms with the two chosen coordinate systems. After the unitary transformation, the atoms are reduced to two-level systems with γ_0 the single-atom spontaneous decay of the first excited state $|e\rangle$ to the ground state $|g\rangle$. All atoms are assumed to have identical transition dipole moments $\mathbf{d}_{eg}$ aligned along the z direction.

from the dependence of the emission dynamics of the Dicke states on the relative orientation of the atomic dipole moments to the wave vector of the exciting photon. Note that we could not identify collective phenomena in very large volumes by our numerical calculation since the atom number is limited to about 10^4. For large volumes, the atomic density is then so low that the emission approaches the single-atom spontaneous emission.

ACKNOWLEDGMENTS

We thank Yan-Jun Chen, Peng Zhang, and Xiang Gao for helpful discussions. This work was supported by the National Natural Science Foundation of China under Grants No. 11174026, No. 11174027, and No. 11174198, and the Research Funds of Renmin University of China (Grant No. 10XNL016).

APPENDIX: CALCULATION OF Eqs. (27) AND (28)

In this Appendix, we provide details of the angular integration required for the calculation of Eqs. (27) and (28). As shown in Fig. 6, we assume the N atoms to be located randomly in space with all dipole moments $\mathbf{d}_{eg}$ aligned along $\hat{e}_z$. For a given pair of two atoms j and j', we denote the direction of $\mathbf{r}_{jj'}$ as $\hat{r}_{jj'} = (\theta_{jj'},\phi_{jj'})$. To simplify the angular integration, we define a new basis $\hat{e}'_{x,y,z}$ such that $\hat{r}_{jj'} \equiv \hat{e}'_z$, $\hat{d}_{eg} = (\theta_{jj'},0)$, and $\hat{k} = (\theta,\phi)$ in the new basis. Thus, $\hat{d}_{eg}$ is in the plane spanned by $\hat{e}'_x$ and $\hat{e}'_z$. The direction of the polarization $\hat{e}_{\mathbf{k}}$ is in the plane spanned by $\hat{k}$ and $\hat{d}_{eg}$.

Then the angle between $\hat{d}_{eg}$ and $\hat{k}$, which we denote as θ_d, satisfies

$$\cos\theta_d = \cos\theta\cos\theta_{jj'} + \sin\theta\cos\phi\sin\theta_{jj'}. \tag{A1}$$

In Eq. (25), the integral over the solid angle for fixed $|\mathbf{k}|$ then gives

$$\begin{aligned}\int_0^{2\pi} d\phi \int_0^{\pi} d\theta \sin\theta g^2_{\mathbf{k},eg} &= g^2_{k,eg}\int_0^{2\pi} d\phi \int_0^{\pi} d\theta \sin\theta \sin\theta_d^2 \\ &= \frac{8\pi}{3} g^2_{k,eg}.\end{aligned} \tag{A2}$$

Further performing the integral over $|\mathbf{k}|$ in Eq. (25) with standard methods, one obtains

$$\Gamma_0 \approx \gamma_0 - i\frac{2\gamma_0}{\pi}. \tag{A3}$$

To obtain this result, we replaced ω'_{eg} in the denominator in Eq. (25) by ω_{eg}. Here, $\gamma_0 \equiv \omega^3_{eg}d^2_{eg}/(3\pi\epsilon_0 c^3) = k^3_{eg}d^2_{eg}/(3\pi\epsilon_0)$ is the standard single-atom decay rate of spontaneous emission, and γ_0/π, which comes from the corresponding imaginary part, is the single-atom Lamb shift.

In Eq. (26), the integral over the solid angle for fixed $|\mathbf{k}|$ gives

$$\begin{aligned}&\int_0^{2\pi} d\phi \int_0^{\pi} d\theta \sin\theta g^2_{\mathbf{k},eg}\cos(\mathbf{k}\cdot\mathbf{r}_{jj'}) \\ &= 2\pi g^2_{k,eg}\int_0^{\pi} d\theta \sin\theta \sin\theta_d^2 \cos(kr_{jj'}\cos\theta) \\ &= \sin^2\theta_{jj'}\left[2\pi g^2_{k,eg}\frac{2\sin kr_{jj'}}{kr_{jj'}}\right] + \frac{(3\cos^2\theta_{jj'}-1)}{2} \\ &\quad\times\left[2\pi g^2_{k,eg}\frac{4\sin kr_{jj'} - 4kr_{jJ}\cos kr_{jj'}}{(kr_{jJ})^3}\right].\end{aligned} \tag{A4}$$

Then, after the integration over $|\mathbf{k}|$, the term $\Gamma^{(j)}_{j'}$ in Eq. (26) can be evaluated to

$$\Gamma^{(j)}_{j'} = \sin^2\theta_{jj'}\Gamma^{(j)}_{j',1} + \frac{(3\cos^2\theta_{jj'}-1)}{2}\Gamma^{(j)}_{j',2}, \tag{A5}$$

where

$$\Gamma^{(j)}_{j',1} = i\frac{3\exp(i\zeta_{jj'})}{2\zeta_{jj'}}\gamma_0 \tag{A6}$$

and

$$\begin{aligned}\Gamma^{(j)}_{j',2} = -\frac{3}{\zeta^3_{jj'}}\gamma_0[&(\sin\zeta_{jj'} - \zeta_{jj'}\cos\zeta_{jj'}) \\ &+ i(1-\cos\zeta_{jj'} - \zeta_{jj'}\sin\zeta_{jj'})]\end{aligned} \tag{A7}$$

with $\zeta_{jj'} := k_{eg}r_{jj'} \equiv \omega_{eg}r_{jj'}/c$.

[1] M. Kiffner, M. Macovei, J. Evers, and C. H. Keitel, *Vacuum-Induced Processes in Multi-Level Atoms*, edited by E. Wolf, Progress in Optics Vol. 55 (Elsevier, Amsterdam, 2010).

[2] R. H. Dicke, Phys. Rev. **93**, 99 (1954).

[3] R. H. Lehmberg, Phys. Rev. A **2**, 883 (1970); **2**, 889 (1970).

[4] N. E. Rehler and J. H. Eberly, Phys. Rev. A **3**, 1735 (1971).

[5] N. Skribanowitz, I. P. Hermann, J. C. MacGillivray, and M. S. Feld, Phys. Rev. Lett. **30**, 309 (1973).
[6] J. C. MacGillivray and M. S. Feld, Phys. Rev. A **14**, 1169 (1976).
[7] Y. Kagan, Hyperfine Interact. **123**, 83 (1999).
[8] M. O. Scully and A. A. Svidzinsky, Science **325**, 1510 (2009); **328**, 1239 (2010).
[9] R. Röhlsberger, K. Schlage, B. Sahoo, S. Couet, and R. Rüffer, Science **328**, 1248 (2010).
[10] A. Pálffy, C. H. Keitel, and J. Evers, Phys. Rev. Lett. **103**, 017401 (2009).
[11] M. Macovei, J. Evers, and C. H. Keitel, Phys. Rev. Lett. **91**, 233601 (2003).
[12] M. Macovei, J. Evers, and C. H. Keitel, Phys. Rev. A **71**, 033802 (2005).
[13] C. Greiner, B. Boggs, and T. W. Mossberg, Phys. Rev. Lett. **85**, 3793 (2000).
[14] F. W. Cummings, Phys. Rev. A **33**, 1683 (1986).
[15] S. Prasad and R. J. Glauber, Phys. Rev. A **61**, 063814 (2000).
[16] I. E. Mazets and G. Kurizki, J. Phys. B **40**, F105 (2007).
[17] M. O. Scully, E. S. Fry, C. H. Raymond Ooi, and K. Wódkiewicz, Phys. Rev. Lett. **96**, 010501 (2006).
[18] A. A. Svidzinsky, J.-T. Chang, and M. O. Scully, Phys. Rev. Lett. **100**, 160504 (2008); A. Svidzinsky and J.-T. Chang, Phys. Rev. A **77**, 043833 (2008), and references therein.
[19] M. O. Scully, Phys. Rev. Lett. **102**, 143601 (2009).
[20] A. A. Svidzinsky, J.-T. Chang, and M. O. Scully, Phys. Rev. A **81**, 053821 (2010).
[21] R. Friedberg and J. T. Manassah, Phys. Lett. A **372**, 2514 (2008); **374**, 1648 (2010).
[22] T. Bienaimé, N. Piovella, and R. Kaiser, Phys. Rev. Lett. **108**, 123602 (2012).
[23] H. Zheng, S.-Y. Zhu, and M. S. Zubairy, Phys. Rev. Lett. **101**, 200404 (2008).
[24] B. Misra and E. C. G. Sudarshan, J. Math. Phys. **18**, 756 (1977).
[25] A. G. Kofman and G. Kurizki, Nature (London) **405**, 546 (2000).
[26] D.-W. Wang, A.-J. Li, L.-G. Wang, S.-Y. Zhu, and M. S. Zubairy, Phys. Rev. A **80**, 063826 (2009).
[27] D.-W. Wang, L.-G. Wang, Z.-H. Li, and S.-Y. Zhu, Phys. Rev. A **80**, 042101 (2009).
[28] Z.-H. Li, D.-W. Wang, H. Zheng, S.-Y. Zhu, and M. S. Zubairy, Phys. Rev. A **80**, 023801 (2009).
[29] D.-W. Wang, Z.-H. Li, L.-G. Wang, S.-Y. Zhu, and M. S. Zubairy, Opt. Lett. **35**, 2861 (2010).
[30] Z.-H. Li, D.-W. Wang, H. Zheng, S.-Y. Zhu, and M. S. Zubairy, Phys. Rev. A **82**, 050501 (2010).
[31] S. Yang, H. Zheng, R. Hong, S.-Y. Zhu, and M. S. Zubairy, Phys. Rev. A **81**, 052501 (2010).
[32] Q. Ai, Y. Li, H. Zheng, and C. P. Sun, Phys. Rev. A **81**, 042116 (2010).
[33] X. Cao, Q. Ai, C. P. Sun, and F. Nori, Phys. Lett. A **376**, 349 (2012).
[34] J. Xu, S. Yang, X.-M. Hu, and M. S. Zubairy, Phys. Lett. A **376**, 297 (2012).
[35] Y. B. Dong, Z. H. Li, Y. Li, and Shi-Yao Zhu, Phys. Rev. A **85**, 013832 (2012).
[36] D.-W. Wang, Z.-H. Li, H. Zheng, and S.-Y. Zhu, Phys. Rev. A **81**, 043819 (2010).
[37] H. A. Bethe, Phys. Rev. **72**, 339 (1947).
[38] M. O. Scully and M. S. Zubairy, *Quantum Optics* (Cambridge University Press, Cambridge, 1997).
[39] Here $L_0 = -\gamma_0/\pi$ is equivalent to the dynamic Lamb shift in the long-time (Markov) limit as given in Ref. [28] [cf. Eq. (C2) therein with i and j being replaced by the first excited state e and the ground state g, respectively].